Computer Networks 160 (2019) 65–76

Contents lists available at ScienceDirect

Computer Networks

journal homepage: www.elsevier.com/locate/comnet

A high-throughput wireless-powered relay network with joint time and power allocations

Gaofei Huang[a,*], Wanqing Tu[b]

[a] Faculty of Mechanistic and Electric Engineering, Guangzhou University, Guangzhou, China
[b] School of Computer Science, The University of Auckland, Auckland 1142, New Zealand

ARTICLE INFO

Article history:
Received 24 December 2018
Revised 24 April 2019
Accepted 5 June 2019
Available online 8 June 2019

Keywords:
Radio-frequency (RF) energy harvesting
Simultaneous wireless information and power transfer (SWIPT)
Relay
Dynamic programming

ABSTRACT

This paper studies how to maximise the throughput for a wireless-powered relay network where an unreliable direct link exists between a source node and a destination node. Our idea is to optimally combine time allocations (for different relay activities) and power allocations (for the relay to forward different frames) based on a harvest-store-consume (HSC) model. With the HSC model, the network may operate in a direct transmission (DT) mode or a cooperative transmission (CT) mode to transmit one frame. Accordingly, the relay may either harvest energy from the radio-frequency signals in the direct link in DT mode, or harvest energy and forward information in CT mode, where the energy harvested in both modes is stored temporarily before it is consumed for information relaying. Moreover, in our CT mode, the relay distributes the energy to the transmissions of multiple consecutive frames by taking time-varying wireless channel conditions in a time period into account in order to achieve the best throughput performance. We formulate a deterministic optimization problem and a stochastic programming problem under the assumption of full channel state information (CSI) and causal CSI, respectively. Both problems optimally determine DT or CT modes for each frame transmission. In the CT mode, the problems also decide the time-switching (TS) ratios and the transmit power at the relay. Our formulated problems are intractable due to the energy distribution at the relay between multiple frames. This intractability is addressed by dynamic programming techniques which decompose the problems into two tractable subproblems: an outer problem, and an inner problem. By solving the two subproblems, we propose the joint TS operation and power allocation algorithms for the two original formulated problems. The proposed algorithm for causal CSI is an online algorithm with low complexity, while the proposed algorithm for full CSI is offline and provides a benchmark for the online algorithm.

1. Introduction

Many wireless devices are energy-constrained wireless nodes. In order to extend the lifetime of these communication devices, studies have investigated simultaneous wireless information and power transfer (SWIPT) schemes in various wireless communication scenarios [1–9], allowing wireless devices to harvest energy from radio-frequency (RF) signals when they receive information. More specifically, in a wireless relay network with SWIPT, the relay node with RF energy-harvesting (EH) capability can not only receive information but also harvest energy via the RF signals emitted by the source. By using the harvested energy, the relay can be powered to forward information the destination, extending the lifetime of its batteries.

1.1. Related works

Wireless-powered relaying has been studied for different wireless relay networks in recent years [10–24]. However, most studies have focused on a topology where a direct link between the source and the destination does not exist [10–22]. In practice, a direct link usually exists in a wireless relay network, although such a link may not perform well due to obstacles etc. With the existence of the direct link, when the source sends information to the destination directly, the relay may harvest energy from the RF signals in the direct link. However, it is not a trivial task to make a decision for the relay when to participate in the cooperative transmissions between the source and the destination. On one hand, if a small portion of time within a period is allocated to direct transmission, the relay harvests a small amount of energy and the performance

* Corresponding author.
E-mail addresses: huanggaofei@gzhu.edu.cn (G. Huang), w.tu@auckland.ac.nz (W. Tu).

https://doi.org/10.1016/j.comnet.2019.06.005
1389-1286/

of WPRN achieved by information relaying may be degraded instead of being improved since the relay forwards information with repetition coding strategy in two orthogonal phases of one frame transmission. On the other hand, if a large portion of time in a period is allocated to direct transmission, few information transmissions take place via the relay link. This results in that the achieved throughput is similar to that only achieved by direct transmission. Therefore, by taking the direct link into account, it is more complicated and challenging to implement design and analysis for the wireless-powered relay network (WPRN).

Related studies have been carried out on such WPRNs recently. In [23], the authors study the WPRN with a direct link by using a harvest-then-forward (HTF) model, which is an energy consumption model based on the popularly studied conventional time-switching relaying (TSR) or power-splitting relaying (PSR) protocol [10]. In the HTF model, the relay firstly employs a time-switching (TS) or power-splitting (PS) EH receiver to harvest energy, and then uses up all available energy for each frame transmission. In order to improve the throughput performance, the work [23] optimizes the TS ratios and the PS ratios for TSR-based and PSR-based WPRNs with rateless coding technology. However, the HTF model has two major drawbacks. Firstly, the harvested energy, only from a portion of the RF energy emitted by sending a frame, is too limited to gain significant performance improvement. Secondly, the relay is restricted to use up all harvested energy for each frame transmission. In fact, if the relay-to-destination (RD) link quality is poor, the energy can be utilized inefficiently as the transmission quality via such a link is not acceptable anyway.

To overcome the drawback that the amount of harvested energy is quite small in the HTF model, the work [24] studies a WPRN with a direct link based on an accumulate-then-forward (ATF) model, where the relay assists in forwarding information only when the harvested energy reaches a predefined energy threshold and the destination fails to decode the information received from the source. However, the scheme makes the relay to transmit without considering the channel condition of the RD link, which is similar to that in the HTF model and may cause that the harvested energy is utilized inefficiently.

1.2. Motivations

To address the drawbacks of the ATF and HTF models, we investigate how to optimally utilize both direct transmission and wireless-powered relaying for the WPRN in this paper. Our goal is to achieve the best average throughput performance in a time period for transmitting multiple frames. To achieve our goal, our idea is to optimally allocate time between direct transmission and wireless-powered relaying within a period of multiple frames by employing a new energy consumption model, namely harvest-store-consume (HSC) model, which is different from the ATF and HTF models. The HSC model was first studied in [25] in a point-to-point wireless communication system where a source node harvests energy from environment (e.g., solar energy) and then reserves the energy for better use in the future. With the HSC model, the relay in our WPRN can store the harvested energy temporarily when the source sends information to the destination directly, i.e., the WPRN can operate in a direct transmission (DT) mode. Moreover, when the source sends information to the destination via the relay, the relay can adjust the amount of energy consumed for the transmission of one frame according to the channel conditions of the WPRN in a time period which includes consecutive multiple frame transmissions, instead of using up all available energy for each transmission. Therefore, compared with that in the ATF or HTF model, the relay in the HSC model can harvest and consume energy more flexibly, and thus the performance of the WPRN may be potentially improved.

In this paper, we assume that the relay is equipped with a TS EH receiver, since the current commercial circuits are designed to deliver information and harvest energy separately [26]. Accordingly, the WPRN can operate in DT mode or cooperative transsmission (CT) mode by enabling the relay to harvest energy or cooperate in information relaying in a TS fashion. We investigate how to jointly optimize the TS operation and transmit power at the relay, which enables the relay to efficiently collect energy and then optimally distribute the stored energy to the transmissions of different frames, eventually helping to maximize the throughput of WPRNs.

1.3. Contributions

In the design of joint time and power allocations for the WPRN with a direct link, our contributions are concluded below.

- We derive the upper bound of the throughput performance for a WPRN with a direct link. This bound is achieved in an offline manner by computer evaluations, where full channel state information (CSI) are generated according to the statistical information of the wireless channels before information transmissions. Because non-causal CSI is required, it is impractical. Nevertheless, it provides a benchmark for the performance which can be achieved in the case of causal CSI. The formulated optimization problem is to optimally determine DT or CT mode for the WPRN and the TS ratios at the EH receiver and transmit power at the relay in CT mode. It is deterministic but challenging to be solved as the involved energy scheduling at the relay is coupled over multiple frame transmissions. We employ dynamic programming and problem decomposition techniques to decouple it in time to obtain two subproblems: an outer problem, and an inner problem, which can be solved by a brute force approach and a two-level optimization approach, respectively.
- We design an online algorithm for the practical case in which only causal CSI is available. The formulated problem, more difficult than the deterministic problem with full CSI, is a stochastic program. Based on the derivation of the offline algorithm, by using a finite-state Markov channel (FSMC) model [31], we derive a low-complexity online algorithm. This algorithm allows our network to obtain a throughput close to the upper bound of the offline algorithm.
- We then use computer simulations to verify our theoretical studies. Our evaluation suggests that the throughput achieved by our algorithm is much higher than that based on the ATF or HTF model. Moreover, our evaluation also observes that the throughput can be improved significantly by efficiently ultilizing the direct link in the WPRN.

The rest of the paper is organized as follows. Section 2 describes our WPRN with the HSC model. Section 3 designs the algorithm that achieves joint time switching and power allocation based on full CSI. Section 4 is about the algorithm achieving joint time switching and power allocation based on causal CSI. Simulation results are shown in Section 5. Section 6 concludes the paper.

2. System model

We consider a three-node two-hop WPRN as shown in Fig. 1. The source node (N1) sends information to the destination node (N3) via the EH relay (N2) that is equipped with a TS receiver. The three nodes are equipped with a single antenna and operate in a half-duplex manner. We assume that the direct link between the source and the destination exists but it is unreliable due to obstacles, which is more practical than the scenario which assumes such a direct link does not exit. The source is powered by fixed supply, but the EH relay is powered by batteries. To prolong the life of the

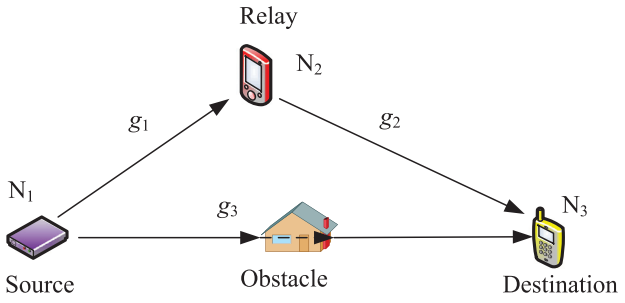

Fig. 1. A two-hop wireless-powered relay network with unreliable direct link.

batteries, the relay only consumes the energy which is harvested from the RF signals emitted by the source while forwarding information to the destination. Moreover, to enable the relay to operate with the HSC model, we assume that the relay is equipped with a rechargeable battery or a supercapacitor to store the energy temporarily, which will be consumed later. Note that circuit power consumed by information decoding at the relay cannot be ignored in practice, since the circuit power reduces the net harvested energy that can be stored in the battery for future use [26,27]. Nevertheless, to simplify the expression of transmission strategy derivation and shed light on how the direct link affects the network performance, we assume that the circuit power can be ignored, which is also adopted in [10–24]. We will demonstrate that the development of our transmission algorithm for the WPRN can be easily extended to the scenario where the circuit power is taken into account (see Remark 1 at the end of Section 2.4). Meanwhile, with the current studies on multi-antenna devices, based on [6–8], we believe that the performance of wireless powered networks can be further improved. We will verify this insight in our future study.

2.1. HSC-based cooperative transmission

With the HSC model, the whole process of communication in the considered WPRN takes place on a time period basis. Each time period includes the transmissions of K frames, whose indexes belong to a set denoted as $\mathcal{K} \triangleq \{1, \cdots, K\}$, and all frame transmissions are of the same duration T_f. The structure of each frame can be one of the two types as illustrated in Fig. 2. The first type is corresponding to the DT mode for the WPRN, where the source directly transmits information to the destination, while the relay harvests energy from the RF signals over the direct link and stores the energy in the rechargeable device. The second type is corresponding to the CT mode, where one frame is divided into three phases. In the first phase, the source, the relay and the destination perform the same operations as those in DT mode, respectively. In the second phase, the source broadcasts information, while both the relay and the destination receive and decode the information. In the third phase, both the source and the relay cooperatively transmit information to the destination. We denote the ratios of the three phases in frame k as $\lambda_1(k)$, $\lambda_2(k)$ and $\lambda_3(k)$, respectively, where $k \in \mathcal{K}$. Let $\boldsymbol{\lambda}(k) = \{\lambda_1(k), \lambda_2(k), \lambda_3(k)\}$ and define $\Lambda(k) \triangleq \left\{\boldsymbol{\lambda}(k) \middle| \sum_{i=1}^{3} \lambda_i(k) = 1, \lambda_i(k) \in [0,1], i \in \{1,2,3\}\right\}$. Note that with HSC model, the relay may consume a portion of the harvested energy to transmit, which means that some energy can be stored in the rechargeable device for future usage after each transmission at the relay.

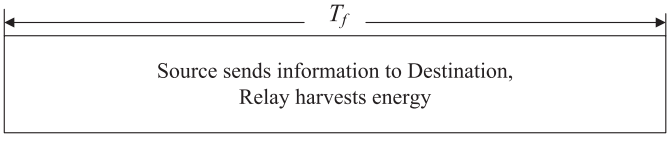

(a) Frame structure in DT mode

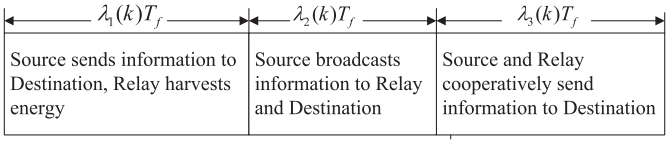

(b) Frame structure in CT mode

Fig. 2. Structures of frames transmitted by the DT mode and the CT mode.

To achieve superior throughput performance in the WPRN, we assume that rateless coding technique is adopted when the WPRN operates in CT mode. That is, the source and the relay need to encode the information with rateless codes before they transmit to the destination. Moreover, similar to the related works on rateless coding based wireless relay networks [23,28,29], we assume that CDMA is employed. Then, in the second phase, the source transmit the encoded information to the relay and destination with its assigned spreading code, while the relay and the destination respectively try decoding the information by accumulating mutual information from the information stream received from the source. When the entropy of original information is marginally surpassed by the collected coded bits, the original information can be successfully decoded and recovered at the relay and the destination [23,28,29]. As the WPRN operates in CT mode, the quality of the source-to-relay link must be better than that of the direct link such that the relay can successfully decode the information before the destination, which will be proved later (see Proposition 1). After the relay decodes the information, it re-encodes the information with a rateless code and transmits it to the destination in the third phase. Meanwhile, the source continuously transmits information to the destination, since CDMA is employed and the orthogonal transmissions between the source and the relay in the third phase can be realized.

Based on the received signals in the second and third phases, the destination may decode the information with the energy-accumulation (EA) method or the information-accumulation (IA) method [23,28,29]. For the EA-based receiving method, the source and the relay use the same spreading code and the same rateless code, while the destination employs the Rake receiver to receive information based on maximal ratio combining method. For the IA-based receiving method, the source and the relay use different spreading codes and independent rateless codes, while the destination can separate the information from the source and the relay to accumulate information. In this paper, we assume that the EA method is adopted, and the results derived in this paper can be easily extended to the WPRN where the IA method is adopted.

We let $\theta(k)$ be indicator of WPRN operation mode. That is, we set $\theta(k) = 0$ for the WPRN in DT mode and $\theta(k) = 1$ for the WPRN in CT mode. Accordingly, the relay can determine its TS operation according to the values of $\theta(k)$ and $\boldsymbol{\lambda}(k)$, $\forall k \in \mathcal{K}$. Specially, consider two adjacent frames, e.g., frame k and frame $(k+1)$ for $k \in \mathcal{K}^o \triangleq \{1, \cdots, K-1\}$. Then, the TS operation at the EH receiver of the relay can happen as the following four cases:

1) $\theta(k) = \theta(k+1) = 0$, which means that the WPRN operates in DT mode in both of the two adjacent frames. In this case, the EH receiver only harvests energy, and thus TS operation does not happen. We illustrate this case in Fig. 3(a).
2) $\theta(k) = 0$ and $\theta(k+1) = 1$, which means that the WPRN operates in DT mode and CT mode in frame k and frame $(k+1)$, respectively. In this case, the EH receiver switches its operation at the end of the first and second phases in frame $(k+1)$ based on the value of $\boldsymbol{\lambda}(k+1)$. We illustrate this case in Fig. 3(b).

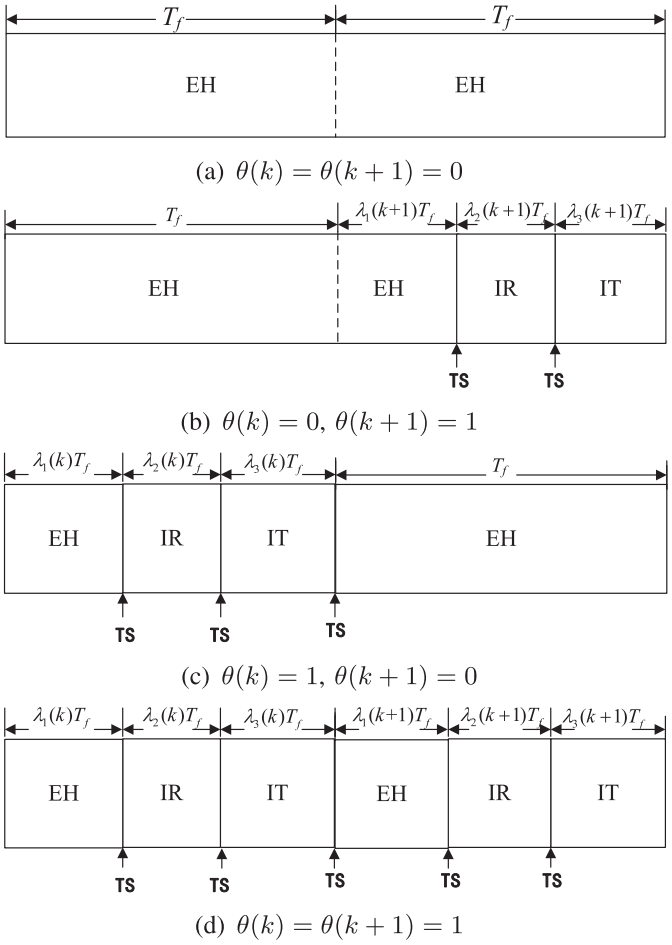

Fig. 3. TS operation in two adjacent frames at the EH receiver of the relay for different $\theta(k)$ and $\theta(k+1)$ (IR: information reception; IT: information transmission).

3) $\theta(k) = 1$ and $\theta(k+1) = 0$, which means that the WPRN operates in CT mode and DT mode in frame k and frame $(k+1)$, respectively. In this case, the EH receiver switches its operation at the end of the three phases in frame k based on the value of $\boldsymbol{\lambda}(k)$. We illustrate this case in Fig. 3(c).
4) $\theta(k) = \theta(k+1) = 1$, which means that the WPRN operates in CT mode in both of the two adjacent frames. In this case, the EH receiver switches its operation at the end of each phase in both of the two adjacent frames based on the values of $\boldsymbol{\lambda}(k)$ and $\boldsymbol{\lambda}(k+1)$. We illustrate this case in Fig. 3(d).

To enable the HSC-based cooperative transmission, the structure of the relay node is illustrated in Fig. 4. According to Fig. 4, there are two switches, i.e., S_1 and S_2, to implement the TS operations between EH and information process at the relay, which is determined by the output of the TS decision unit, i.e., O_1 and O_2. When the relay harvests energy, S_1 switches to the EH branch and S_2 is opened, which results in that the havested energy is stored in the battery. When the relay receives and forwards information, S_1 switches to the transceiver branch and S_2 is closed. Meanwhile, the TS operations between information receiving and information forwarding are determined by the output O_3 of the TS decision unit, i.e., the values of $\lambda_2(k)$ and $\lambda_2(k)$ when the relay operates in CT mode in frame k.

2.2. Channel model

We assume that the channels in the WPRN are quasi-static fading. That is, the channel coefficients remain constant in the duration of one frame, but are i.i.d. for different frames. For frame k, denote the channel coefficient of the link between the source and the relay as $a_1(k)$, denote the channel coefficient of the link between the relay and the destination as $a_2(k)$, and denote the channel coefficient of the link between the source and the destination as $a_3(k)$. The corresponding channel gain is expressed as $g_i(k) = |a_i(k)|^2$, where $i \in \{1, 2, 3\}$. Denote the received additive white Guassian noise (AWGN) power at the relay and the destination as $\sigma_2^2(k)$ and $\sigma_3^2(k)$, respectively. Then, the normalized channel gain of $g_1(k)$ is expressed as $G_1(k) = \frac{g_1(k)}{\sigma_2^2(k)}$, and the normalized channel gains of $g_2(k)$ and $g_3(k)$ are expressed as $G_2(k) = \frac{g_2(k)}{\sigma_3^2(k)}$ and $G_3(k) = \frac{g_3(k)}{\sigma_3^2(k)}$, respectively.

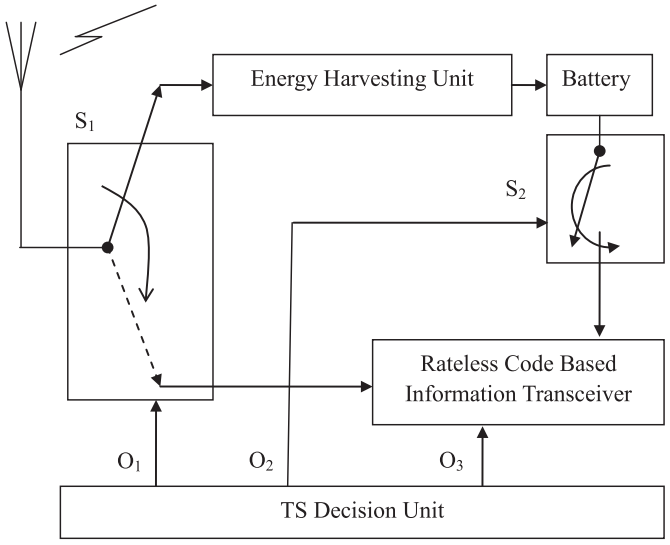

Fig. 4. Structure of the HSC-based relay.

In this paper, we consider two scenarios for the knowledge of CSI at the transmitters. Firstly, we consider an ideal scenario, where the transmitters have the knowledge of full CSI of K frames at the beginning of the first frame transmission in a period, which indicates that non-causal CSI is available. Then, we consider a practical scenario, where the transmitters have only the knowledge of current CSI before transmission, which indicates that only causal CSI is available. Moreover, for the second scenario, we assume that the statistics, i.e., probability density functions (pdfs), of the channels in the WPRN have been known.

2.3. Definition of throughput for the WPRN

In the considered WPRN, we assume that the source transmits with constant power, i.e., P_1, for all frames. Then, we can obtain the achievable end-to-end data rate for the WPRN in DT mode as $R_{\mathrm{DT}}(k) = R_3(k) = \log(1 + P_1 G_3(k))$. Moreover, we can obtain the achievable data rate from the source to the relay as $R_1(k) = \log(1 + P_1 G_1(k))$. Denote the transmit power of the relay in frame k as $p_2(k)$. Then, as the EA method is adopted, the achievable data rate in the cooperative transmission from the source and the relay to the destination can be expressed as

$$R_{\mathrm{c}}(k) = \log(1 + P_1 G_3(k) + p_2(k) G_2(k)). \tag{1}$$

Furthermore, for CT mode, we can obtain the data rate which can be achieved in the WPRN in frame k as [29]

$$R_{\mathrm{CT}}(k) = \min\{\lambda_2(k) R_1(k), [\lambda_1(k) + \lambda_2(k)] R_3(k) + \lambda_3(k) R_{\mathrm{c}}(k)\}. \tag{2}$$

Then, we can express the average throughput over one period, which includes K consecutive frame transmissions, for the WPRN as

$$\mathcal{T} = \frac{1}{K}\sum_{k=1}^{K}[(1-\theta(k))R_{\mathrm{DT}}(k) + \theta(k)R_{\mathrm{CT}}(k)]. \tag{3}$$

2.4. Energy scheduling constraint at the relay

With the HSC model, we can schedule the energy consumption across multiple frames at the relay when the WPRN operates in CT mode. Denote the energy utilization efficiency as $\eta \in (0, 1)$. Then, when the WPRN operates in DT mode in frame k, the amount of harvested energy is calculated as $E_{\mathrm{DT}}(k) = \eta T_f P_1 g_1(k)$. When the WPRN operates in CT mode in frame k, the relay harvests energy in the first phase, and the amount of harvested energy is calculated as $E_{\mathrm{CT}}(k) = \eta\lambda_1(k)T_f P_1 g_1(k)$. Thus, in frame k, the amount of available energy can be calculated as [29]

$$\begin{aligned} E(k) &= (1-\theta(k))E_{\mathrm{DT}}(k) + \theta(k)E_{\mathrm{CT}}(k) \\ &= V(k)[(1-\theta(k)) + \theta(k)\lambda_1(k)], \end{aligned} \tag{4}$$

where $V(k) = \eta T_f P_1 g_1(k)$.

Denote the time instant just before frame k as k^-. Furthermore, at time instant k^-, denote the amount of available energy at the rechargeable device as $B(k) \geq 0$, which can be measured at the relay. Then, the energy scheduling constraint at the relay in frame k can be written as [29]

$$\sum_{t=1}^{k} T_f\theta(t)\lambda_3(t)p_2(t) \leq \min\left\{B(1) + \sum_{t=1}^{k}E(t), B_{\max}\right\}, \ \forall k \in \mathcal{K}, \tag{5}$$

where $B_{\max}$ is the maximum allowable stored energy in the rechargeable device at the relay.

Remark 1. As mentioned previously, we ignore the circuit power at the relay in this paper. When the circuit power is taken into account, the energy available for information relaying decreases, which causes the achievable end-to-end data rate of CT mode decreases, and the WPRN may opt to operate in DT mode in more frames within one time period. To obtain the corresponding transmission strategy, we just need to modify the energy scheduling constraint in (5) as

$$\begin{aligned} &\sum_{t=1}^{k} T_f\theta(t)[\lambda_3(t)p_2(t) + P_c] \\ &\quad \leq \min\left\{B(1) + \sum_{t=1}^{k}E(t), B_{\max}\right\}, \ \forall k \in \mathcal{K}, \end{aligned} \tag{6}$$

where the constant P_c is the circuit power consumption at the relay when the WPRN operates in CT mode. Since only a constant is appended in the constraint, it can be easily verified that the derivation of the optimization algorithms presented in Sections 3 and 4 can be extended to the scenario where the circuit power is taken into account.

3. Offline joint TS operation and power allocation algorithm

In this section, we assume that the full CSI of K frames over one period has been known before transmission. Although it is an ideal scenario, the derived offline joint TS operation and power allocation algorithm can provide a benchmark for the practical scenario where only causal CSI is known.

3.1. Problem formulation

In this paper, we aim at maximizing the average throughput, which is defined in (3), by optimizing the TS operation and power allocation over one period. We denote the variables to be optimized as $\Xi(k) = \{\theta(k) \in \{0, 1\}, p_2(k) \geq 0, \boldsymbol{\lambda}(k) \in \Lambda(k)\}$. As the full CSI of K frames in one period has been known, we can formulate the optimization problem as

$$\max_{\Xi(k), \forall k \in \mathcal{K}} \sum_{k=1}^{K}[(1-\theta(k))R_{\mathrm{DT}}(k) + \theta(k)R_{\mathrm{CT}}(k)] \tag{7a}$$

$$\text{s.t. } (5). \tag{7b}$$

The energy scheduling constraint (7b) in problem (7) is non-convex due to the product term in the left side. Moreover, problem (7) is coupled over K frames. Thus, problem (7) is hard to solve directly. To make it tractable, we denote a vector of length k as $X^k = [X(1), \cdots, X(k)]$ in general, e.g., the energy of the rechargeable device at the relay from frame 1 to frame k is expressed as $B^k = [B(1), \cdots, B(k)]$. Then, at frame $(k+1)^-$, the stored energy is updated in general as

$$B(k+1) = f(B^k, p_2^k, \boldsymbol{\lambda}^k). \tag{8}$$

Then, we can also rewrite the energy scheduling constraint (7b) as

$$T_f\theta(k)\lambda_3(k)p_2(k) \leq \min\{B(k) + E(k) - B(k+1), B_{\max}\} \tag{9}$$

for $k \in \mathcal{K}^o$ and

$$T_f\theta(K)\lambda_3(K)p_2(K) \leq \min\{B(K) + E(K), B_{\max}\}. \tag{10}$$

We obtain (10) because the relay will use up all the available energy to transmit when the WPRN operates in CT mode.

Note that $B(k)$ $(k \in \mathcal{K})$ can be measured at the relay before the transmission of frame k, while $B(k+1)$ $(k \in \mathcal{K}^o)$ is a variable to be determined since $p_2(k)$ needs to be optimized. Moreover, according to (9), we have

$$B(k) + E(k) - B(k+1) \geq 0, \tag{11}$$

otherwise the constraint in (9) cannot be satisfied. Thus, we obtain

$$B(k+1) \leq B(k) + E(k) \overset{(a)}{\leq} B(k) + V(k), \tag{12}$$

where (a) holds because we can obtain $E(k) \leq V(k)$ according to (4).

Thus, we let $\Xi'(k) = \Xi(k) \bigcup B(k+1)$, for $k \in \mathcal{K}^o$. Then, according to Bellman equation [32], we can transform problem (7) into the following equations which can equivalently obtain the optimal solutions,

$$\begin{aligned} F^*(B(k), k) = \max_{\Xi'(k)} &(1-\theta(k))R_{\mathrm{DT}}(k) + \theta(k)R_{\mathrm{CT}}(k) \\ &+ F^*(B(k+1), (k+1)), \ \forall k \in \mathcal{K}^o, \\ &\text{s.t. } (9), \end{aligned} \tag{13}$$

$$F^*(B(K), K) = \max_{\Xi(K)} (1-\theta(K))R_{\mathrm{DT}}(K) + \theta(K)R_{\mathrm{CT}}(K) \quad \text{s.t. } (10). \tag{14}$$

To obtain the optimal value of problem (7) by the above equations, we need to solve these equations recursively by using the backward induction method [32]. That is, start from the last Eq. (14) and work backward until the first equation in (13) for $k = 1$. Then, the obtained $F^*(B(1), 1)$ is the same as the optimal value in problem (7).

To solve the equations in (13) and (14), we first derive the decision criteria of optimal network operation mode, i.e., $\theta(k)$ $(k \in \mathcal{K})$, and then obtain the solutions of the other optimized variables in $\Xi'(k)$ $(k \in \mathcal{K}^o)$ and $\Xi(K)$.

3.2. Decision criteria of network operation mode

Recall that the relay performs EH when the WPRN operates in DT mode. Thus, given the energy state $B(k)$ at time instant k^-, the energy state at time instant $(k+1)^-$ can be calculated as $B(k+1)=B(k)+V(k)$. Note that $B(k+1)\in\mathcal{B}$. Thus, $B(k+1)$ should be obtained as the optimal solution, i.e., x^*, to the problem such as follows,

$$\min_{x\in\mathcal{B}} B(k)+V(k)-x,\ \text{s.t. B(k)+V(k)-x}\geq 0. \tag{15}$$

We denote $\tilde{B}(k)=x^*$. Furthermore, define $\tilde{\Xi}(k)=\Xi(k)\backslash\theta(k)$ and $\tilde{\Xi}'(k)=\Xi'(k)\backslash\theta(k)$. Then, the WPRN can determine its optimal operation mode as stated in the following proposition.

Proposition 1. *If $g_3(k)\geq g_1(k)$, the optimal operation mode of the WPRN in frame k ($k\in\mathcal{K}$) is $\theta^*(k)=0$. Otherwise, $\theta^*(k)$ ($k\in\mathcal{K}$) is determined by*

$$\theta^*(k)=\begin{cases}0, & F_{\mathrm{D}}^*(B(k),k)\geq F_{\mathrm{C}}^*(B(k),k)\\ 1, & otherwise\end{cases} \tag{16}$$

in which $F_{\mathrm{D}}^*(B(K),K)=R_{\mathrm{DT}}(K)$, $F_{\mathrm{D}}^*(B(k),k)=R_{\mathrm{DT}}(k)+F^*\left(\tilde{B}(k+1),(k+1)\right)$,

$$F_C^*(B(K),K)=\max_{\tilde{\Xi}(K)} R_{\mathrm{CT}}(K) \tag{17a}$$

$$\text{s.t. } T_f\lambda_3(K)p_2(K)\leq B(K)+\lambda_1(K)V(K) \tag{17b}$$

and

$$F_C^*(B(k),k)=\max_{\tilde{\Xi}'(k)} R_{\mathrm{CT}}(k)+F^*(B(k+1),(k+1)),\forall k\in\mathcal{K}^o, \tag{18a}$$

$$\text{s.t. } T_f\lambda_3(k)p_2(k)\leq B(k)+\lambda_1(k)V(k)-B(k+1). \tag{18b}$$

Proof. See Appendix A. □

To determine the network operation mode by Proposition 1, we need to solve problem (17) and problem (18). Note that if we solve problem (18), we can also solve problem (17) by using the same approach. Thus, we only focus on solving problem (18) in the following subsection, which corresponds to the resource allocations in CT mode.

3.3. Resource allocations in CT mode

Problem (18) is still not easy to solve because the variable $B(k+1)$ is continuous, which makes the number of possible solutions is infinite, and the problem is coupled with two frames, i.e., frame k and frame $(k+1)$. To make it tractable, as in [30], we adopt a discrete model for the energy states of the rechargeable device. That is, the number of energy states is finite, which is denoted as $(L+1)$, and the set of energy states can be defined as $\mathcal{B}\triangleq\left\{0,\frac{B_{\max}}{L},\frac{2B_{\max}}{L},\cdots,B_{\max}\right\}$. Then, $B(k+1)$ should satisfy $B(k+1)\in\mathcal{B}$ and the inequality (12). Thus, we can obtain a feasible set of $B(k+1)$, which is defined as $\widehat{\mathcal{B}}$.

Based on the discrete energy state model, we can decompose problem (18) into two subproblems, namely an inner problem and an outer problem. The inner problem is obtained by fixing $B(k+1)\in\widehat{\mathcal{B}}$ in problem (18), i.e.,

$$Q^*(B(k+1))=\max_{\tilde{\Xi}(k)} R_{\mathrm{CT}}(k)\quad \text{s.t. (18b)}, \tag{19}$$

while the outer problem is to obtain the optimal $B^*(k+1)$, i.e.,

$$F_{\mathrm{CT}}^*(B(k),k)=\max_{B(k+1)\in\widehat{\mathcal{B}}} Q^*(B(k+1))+F^*(B(k+1),(k+1)). \tag{20}$$

We can obtain the optimal value of problem (18) by two steps. The first step is to obtain $Q^*(B(k+1))$ by solving problem (19) for all $B(k+1)$'s, and the second step is to search for the optimal $B^*(k+1)$ in $\widehat{\mathcal{B}}$ by solving problem (20) with the brute force approach.

However, because the energy scheduling constraint (18b) is non-convex, problem (19) is non-convex. Thus, it is still not easy to solve problem (19) directly. To tackle this problem, we propose to solve it by a two-level optimization approach, namely an inner-lever problem and an outer-level problem. The inner-level problem is to fix $\lambda_1(k)$ and search for the optimal $\tilde{\Xi}^*(k)$, where $\tilde{\Xi}(k)=\tilde{\Xi}(k)\backslash\lambda_1(k)$, to the following optimization problem

$$A^*(\lambda_1(k))=\max_{\tilde{\Xi}(k)} R_{\mathrm{CT}}(k)\ \text{s.t. (18b)}. \tag{21}$$

The outer-level problem is to search for the optimal $\lambda_1^*(k)$ to the following optimization problem

$$\max_{\lambda_1(k)\in[0,1]} A^*(\lambda_1(k)). \tag{22}$$

Note that the right-hand side of (18b) (denoted as $W(k)=B(k)+\lambda_1(k)V(k)-B(k+1)$) may be negative for some given $B(k+1)\in\mathcal{B}'$ and $\lambda_1(k)\in[0,1]$. In this case, problem (21) has no feasible solution and we let the optimal value of (21) as $A^*(\lambda_1(k))=0$. Otherwise, we have the following lemma for the achievable data rates in the two phases of one frame transmission in CT mode.

Lemma 1. *Given $\lambda_1(k)\in[0,1]$, the following inequality*

$$\lambda_2(k)R_1(k)\geq[\lambda_1(k)+\lambda_2(k)]R_3(k)+\lambda_3(k)R_{\mathrm{c}}(k) \tag{23}$$

is satisfied when the solution to problem (21) is achieved at optimality.

Proof. See Appendix B. □

According to Lemma 1, we can establish the following proposition.

Proposition 2. *Given $\lambda_1(k)\in[0,1]$ and suppose that $W(k)\geq 0$. When the solution to problem (21) is achieved at optimality, the energy scheduling constraint (18b) is active. That is,*

$$T_f\lambda_3(k)p_2(k)=W(k). \tag{24}$$

Proof. See Appendix C. □

According to (24) in Proposition 2, we can obtain the optimal $p_2(k)$ as

$$p_2(k)=\left[\frac{W(k)}{T_f\lambda_3(k)}\right]^+. \tag{25}$$

Then, we can rewrite problem (21) as

$$A^*(\lambda_1(k))=\max_{\lambda_3(k)\in[0,1]} R'_{\mathrm{CT}}(k), \tag{26}$$

where $R'_{\mathrm{CT}}(k)=\min\left\{\lambda_2(k)R_1(k),[\lambda_1(k)+\lambda_2(k)]R_3(k)+\lambda_3(k)R'_{\mathrm{c}}(k)\right\}$, in which $R'_{\mathrm{c}}(k)=\lambda_3(k)\log\left(1+P_1G_3(k)+\left[\frac{W(k)}{T_f\lambda_3(k)}\right]^+G_2(k)\right)$.

It can be proved that $R'_{\mathrm{CT}}(k)$ is concave in $\lambda_3(k)$. Therefore, problem (26) can be solved by the means of the golden section search technique. Given $\lambda_1(k)$ and according to $\lambda_2(k)=1-\lambda_1(k)-\lambda_3(k)$, the involved algorithm to solve problem (26) is illustrated in Algorithm 1.

Note that $A^*(\lambda_1(k))$ is concave. Therefore, after achieving the optimal value of (26), we can also employ the golden section search technique to solve problem (22). As a result, we illustrate the involved algorithm to solve the inner problem (19) in Algorithm 2.

In summary, as the knowledge of full CSI is available, we can obtain the joint TS operation and power allocation algorithm to achieve the maximum throughput in the WPRN as Algorithm 3, where the input is $B(1)$ and $g_i(k)$, $\forall i\in\{1,2,3\}$, $\forall k\in\mathcal{K}$.

Algorithm 1 Algorithm to Solve Problem (26).

Initialization: Set tolerance $\epsilon > 0$, $\lambda_3^{\min} = 0$, $\lambda_3^{\max} = 1$, $\lambda_3^{\mathrm{U}} = \lambda_3^{\max}$ and $\lambda_3^{\mathrm{L}} = \lambda_3^{\min}$.
while $\lambda_3^{\mathrm{U}} - \lambda_3^{\mathrm{L}} > \epsilon$ **do**
  $\lambda_3^{\mathrm{U}} = \lambda_3^{\min} + (\lambda_3^{\max} - \lambda_3^{\min}) * 0.618$,
  $\lambda_3^{\mathrm{L}} = \lambda_3^{\max} + \lambda_3^{\min} - \lambda_3^{\mathrm{U}}$,
  Use $\lambda_3(k) = \lambda_3^{\mathrm{U}}$ and $\lambda_3(k) = \lambda_3^{\mathrm{L}}$ to calculate $R'_{\mathrm{CT}}(k)$ to obtain $R'_{\mathrm{CT,U}}(k)$ and $R'_{\mathrm{CT,L}}(k)$, respectively,
  if $R'_{\mathrm{CT,U}}(k) > R'_{\mathrm{CT,L}}(k)$ **then**
    $\lambda_3^{\min} = \lambda_3^{\mathrm{L}}$,
  else
    $\lambda_3^{\max} = \lambda_3^{\mathrm{U}}$.
  end if
end while
Calculate $\lambda_3^*(k) = (\lambda_3^{\mathrm{U}} + \lambda_3^{\mathrm{L}})/2$ and $\lambda_2^*(k) = 1 - \lambda_1(k) - \lambda_3^*(k)$, calculate $p_2^*(k)$ according to (25) and obtain $A^*(\lambda_1(k))$.

Algorithm 2 Algorithm to Solve the Inner Problem (19).

Initialization: Set tolerance $\varepsilon > 0$, $\lambda_1^{\min} = 0$, $\lambda_1^{\max} = 1$, $\lambda_1^{\mathrm{U}} = \lambda_1^{\max}$ and $\lambda_1^{\mathrm{L}} = \lambda_1^{\min}$.
while $\lambda_1^{\mathrm{U}} - \lambda_1^{\mathrm{L}} > \varepsilon$ **do**
  $\lambda_1^{\mathrm{U}} = \lambda_1^{\min} + (\lambda_1^{\max} - \lambda_1^{\min}) * 0.618$,
  $\lambda_1^{\mathrm{L}} = \lambda_1^{\max} + \lambda_1^{\min} - \lambda_1^{\mathrm{U}}$,
  Use $\lambda_1(k) = \lambda_1^{\mathrm{U}}$ to calculate $W(k)$ (denoted as $W_{\mathrm{U}}(k)$), and use $\lambda_1(k) = \lambda_1^{\mathrm{L}}$ to calculate $W(k)$ (denoted as $W_{\mathrm{L}}(k)$).
  if $W_{\mathrm{U}}(k) < 0$ **then**
    $A_{\mathrm{U}}^*(\lambda_1(k)) = 0$.
  else
    Employ Algorithm 1 to obtain $A^*(\lambda_1(k))$ (denoted as $A_{\mathrm{U}}^*(\lambda_1(k))$) with $\lambda_1(k) = \lambda_1^{\mathrm{U}}$.
  end if
  if $W_{\mathrm{L}}(k) < 0$ **then**
    $A_{\mathrm{L}}^*(\lambda_1(k)) = 0$.
  else
    Employ Algorithm 1 to obtain $A^*(\lambda_1(k))$ (denoted as $A_{\mathrm{L}}^*(\lambda_1(k))$) with $\lambda_1(k) = \lambda_1^{\mathrm{L}}$.
  end if
  if $A_{\mathrm{U}}^*(\lambda_1(k)) > A_{\mathrm{L}}^*(\lambda_1(k))$ **then**
    $\lambda_1^{\min} = \lambda_1^{\mathrm{L}}$.
  else
    $\lambda_1^{\max} = \lambda_1^{\mathrm{U}}$.
  end if
end while
Obtain $\lambda_1^*(k) = (\lambda_1^{\mathrm{U}} + \lambda_1^{\mathrm{L}})/2$.

As mentioned previously, we cannot achieve the performance by Algorithm 3 in practice, because it requires full CSI, which is non-causal, over one time period before transmission. Nevertheless, we provide a theoretical upper bound on performance of the proposed practical strategy which requires only causal CSI, which will be derived in the next section.

4. Online joint TS operation and power allocation algorithm

In the previous section, we have derived the offline joint TS operation and power allocation algorithm by assuming that the knowledge of full CSI is available, which can achieve an upper bound of the throughput performance in the WPRN. However, in practice, a transmitter cannot know the CSI in subsequent frames before it transmits in some frame. That is, the transmitter has only the causal knowledge of the CSI. Therefore, in this section, we investigate the online joint TS operation and power allocation

Algorithm 3 Algorithm to Achieve the Maximum Throughput in the WPRN with Full CSI.

Set $l = 0$.
while $l \le L$ **do**
  Calculate $B(K) = l\frac{B_{\max}}{L}$ and $F_D^*(B(K), K) = R_{\mathrm{DT}}(K)$.
  if $g_3(K) \ge g_1(K)$ **then**
    Set $\theta^*(K) = 0$.
  else
    Obtain $F_C^*(B(K), K)$ and $\bar{\Xi}^*(K)$ by solving problem (17),
    Obtain $\theta^*(K)$ according to (16).
  end if
  if $\theta^*(K) = 0$ **then**
    Let $F^*(B(K), K) = F_D^*(B(K), K)$ and $\Xi^*(K) = \{\theta^*(K)\}$.
  else
    Let $F^*(B(K), K) = F_C^*(B(K), K)$ and derive $\Xi^*(K)$ from $\bar{\Xi}^*(K)$.
  end if
  Record $\Xi^*(K)|_{B(K)} = \Xi^*(K)$ and set $l = l + 1$.
end while
Set $k = K$ and $l = 0$.
while $k \ge 1$ **do**
  $k = k - 1$.
  while $l \le L$ **do**
    Calculate $B(k) = l\frac{B_{\max}}{L}$ and $F_D^*(B(k), k) = R_{\mathrm{DT}}(k)$.
    if $g_3(k) \ge g_1(k)$ **then**
      Set $\theta^*(k) = 0$.
    else
      Obtain $F_C^*(B(k), k)$ and $\bar{\Xi}^*(k)$ by solving problem (18),
      Obtain $\theta^*(k)$ according to (16).
    end if
    if $\theta^*(k) = 0$ **then**
      Let $F^*(B(k), k) = F_D^*(B(k), k)$ and $\Xi^*(k) = \{\theta^*(k)\}$.
    else
      Let $F^*(B(k), k) = F_C^*(B(k), k)$ and derive $\Xi^*(k)$ from $\bar{\Xi}^*(k)$.
    end if
    Record $\Xi^*(k)|_{B(k)} = \Xi^*(k)$ and set $l = l + 1$.
  end while
end while
Deduce the throughput based on $\Xi^*(1)|_{B(1)}$.

algorithm when the CSI is known causally. Moreover, to utilize the wireless channel variations to improve the throughput performance, we also assume that the pdfs of the channels in the WPRN have been known at the transmitters. To obtain the algorithm, we first formulate the involved problem as a stochastic optimization problem. Then, we adopt a FSMC model [31] to transform the formulated problem into a deterministic form, where an online algorithm with low computational complexity is derived to achieve superior throughput performance in the WPRN.

4.1. Problem formulation

To formulate the throughput maximization problem when only causal CSI is available, we denote the CSI in the WPRN in frame k as $\boldsymbol{g}(k) = \{g_1(k), g_2(k), g_3(k)\}$. Moreover, considering the energy state, i.e., $B(k)$, we define the *state* of the WPRN in frame k as $\boldsymbol{D}(k) = \{\boldsymbol{g}(k), B(k)\}$. Then, because the CSI in subsequent frames is random and cannot be known in advance, the average throughput over a period expressed in (3) should be modified as

$$\bar{\mathcal{T}} = \mathbb{E}\left\{\frac{1}{K}\sum_{k=1}^{K}[(1-\theta(k))R_{\mathrm{DT}}(k) + \theta(k)R_{\mathrm{CT}}(k)]|\boldsymbol{D}(1)\right\}, \tag{27}$$

where the expectation $\mathbb{E}\{\cdot\}$ is performed over all $\boldsymbol{g}(k)$'s in a period. Thus, we can modify the throughput maximization problem in (7) as

$$\max_{\Xi(k),\forall k\in\mathcal{K}} \mathbb{E}\left\{\sum_{k=1}^{K}[(1-\theta(k))R_{\mathrm{DT}}(k)+\theta(k)R_{\mathrm{CT}}(k)]|\boldsymbol{D}(1)\right\} \tag{28a}$$

$$\text{s.t. (5).} \tag{28b}$$

Recall that the energy scheduling constraint (5) can be rewritten as (9) and (10). Thus, similar to that in Section 3.1, we can transform problem (28) into the following equations

$$F^*(\boldsymbol{D}(k),k)=\max_{\Xi'(k)}(1-\theta(k))R_{\mathrm{DT}}(k)+\theta(k)R_{\mathrm{CT}}(k) + \bar{F}^*(\boldsymbol{D}(k+1),(k+1)),\ \forall k\in\mathcal{K}^o, \quad \text{s.t. (9)}, \tag{29}$$

$$F^*(\boldsymbol{D}(K),K)=\max_{\Xi(K)}(1-\theta(K))R_{\mathrm{DT}}(K)+\theta(K)R_{\mathrm{CT}}(K) \quad \text{s.t. (10)}, \tag{30}$$

where

$$\bar{F}^*(\boldsymbol{D}(k+1),(k+1))=\mathbb{E}_{\boldsymbol{g}(k+1)}[F^*(\boldsymbol{D}(k+1),(k+1))]. \tag{31}$$

4.2. Problem transformation with the FSMC model

Although the statistics of $\boldsymbol{g}(k+1)$ is known, it is not easy to obtain $\bar{F}^*(\boldsymbol{D}(k+1),(k+1))$ in (34). Therefore, the equations in (29) and (30) are more difficult to solve than those in (13) and (14). Thus, in the follows, we adopt a FSMC model to transform these equations into deterministic forms, which can make the involved problems tractable.

The FSMC models have been widely used for modeling wireless flat-fading channels in a variety of applications since the mid 1990s, which are versatile, and with suitable choices of model parameters, can capture the essence of time-varying fading channels [31]. By employing the FSMC models, the continuous channel gain can be quantized with a finite number of values, where each value is named as a state. There have been many methods to quantize the channel gains into a finite number of states [31]. Specially, we adopt the equal probable steady state method [31] in this paper, where the steady-state probabilities for all obtained FSMC states are equal. Suppose that the channel gain $\boldsymbol{g}(k)$ is quantized into N states, which are included in a discrete set $\chi(k)=\{\boldsymbol{g}_1(k),\boldsymbol{g}_2(k),\cdots,\boldsymbol{g}_N(k)\}$, and denote the state of $\boldsymbol{g}(k)$ as $\boldsymbol{\xi}(k)=\{\xi_1(k),\xi_2(k),\xi_3(k)\}$, where $\boldsymbol{\xi}(k)\in\chi(k)$. Furthermore, let $\tilde{\boldsymbol{D}}(k)=\{\boldsymbol{\xi}(k),B(k)\}$. Then, we can rewrite the equations in (29) and (30) as

$$F^*\big(\tilde{\boldsymbol{D}}(k),k\big)=\max_{\Xi'(k)}(1-\theta(k))\tilde{R}_{\mathrm{DT}}(k)+\theta(k)\tilde{R}_{\mathrm{CT}}(k) + \bar{F}^*\big(\tilde{\boldsymbol{D}}(k+1),(k+1)\big),\ \forall k\in\mathcal{K}^o,$$
$$\text{s.t. } \mathrm{T_f}\theta(\mathrm{k})\lambda_3(\mathrm{k})\mathrm{p}_2(\mathrm{k})\le\min\left\{\mathrm{B(k)}+\tilde{\mathrm{E}}(\mathrm{k})-\mathrm{B(k+1)},\mathrm{B_{max}}\right\}, \tag{32}$$

$$F^*\big(\tilde{\boldsymbol{D}}(K),K\big)=\max_{\Xi(K)}(1-\theta(K))\tilde{R}_{\mathrm{DT}}(K)+\theta(K)\tilde{R}_{\mathrm{CT}}(K)$$
$$\text{s.t. } \mathrm{T_f}\theta(\mathrm{K})\lambda_3(\mathrm{K})\mathrm{p}_2(\mathrm{K})\le\min\left\{\mathrm{B(K)}+\tilde{\mathrm{E}}(\mathrm{K}),\mathrm{B_{max}}\right\}, \tag{33}$$

where $\tilde{R}_{\mathrm{DT}}(k)$, $\tilde{R}_{\mathrm{CT}}(k)$ and $\tilde{E}(k)$ can be obtained by replacing $\boldsymbol{g}(k)$ with $\boldsymbol{\xi}(k)$ in $R_{\mathrm{DT}}(k)$, $R_{\mathrm{CT}}(k)$ and $E(k)$, respectively.

As the equal probable steady state method is employed, we obtain $p\big(\boldsymbol{\xi}(k+1)\big)=\frac{1}{N^3}$. Note that $\bar{F}^*\big(\tilde{\boldsymbol{D}}(k+1),(k+1)\big)=\sum_{\boldsymbol{\xi}(k+1)}\big[p\big(\boldsymbol{\xi}(k+1)\big)F^*\big(\tilde{\boldsymbol{D}}(k+1),(k+1)\big)\big]$. Thus, we have

$$\bar{F}^*\big(\tilde{\boldsymbol{D}}(k+1),(k+1)\big)=\frac{1}{N^3}\sum_{\boldsymbol{\xi}(k+1)}\big[F^*\big(\tilde{\boldsymbol{D}}(k+1),(k+1)\big)\big]. \tag{34}$$

As $\bar{F}^*\big(\tilde{\boldsymbol{D}}(k+1),(k+1)\big)$ has been derived, we can solve the equations in (32) and (33) by the same approach that we have derived to solve the equations in (13) and (14).

4.3. Joint time switching and power allocation algorithm with causal CSI

As the equations in (32) and (33) can be solved, we can obtain the joint TS operation and power allocation strategy for a given state $\tilde{\boldsymbol{D}}(k)$, $\forall k\in\mathcal{K}$. Note that for $\tilde{\boldsymbol{D}}(k)$, the number of possible values can be $N^3\times(L+1)$. Furthermore, for $\boldsymbol{\mathcal{S}}=\{\tilde{\boldsymbol{D}}(1),\cdots,\tilde{\boldsymbol{D}}(K)\}$ over one period, the number of possible values can be $K\times N^3\times(L+1)$. Therefore, we can establish a look-up table which has $K\times N^3\times(L+1)$ entries, where an entry corresponds to a state $\tilde{\boldsymbol{D}}(k)$. In the entry corresponding to $\tilde{\boldsymbol{D}}(k)$ $(k\in\mathcal{K}^o)$, we record the optimal $\{\theta^*(k),B^*(k+1)\}$. In the entry corresponding to $\tilde{\boldsymbol{D}}(K)$, we record $\{\theta^*(K)\}$. We illustrate the procedure to obtain the optimal network operation mode $\theta^*(k)$ and energy state $B^*(k+1)$ for each state $\tilde{\boldsymbol{D}}(k)$ in Algorithm 4. Note that when $\theta^*(k)=0$ and $k\in\mathcal{K}^o$, we set $B^*(k+1)=$ NULL in the record because the relay only harvests energy and does not need to know the energy state $B^*(k+1)$ when the WPRN operates in DT mode.

Algorithm 4 The Procedure to Obtain the Optimal Network Operation Mode and Energy State under the FSMC Model.

1: Set $l=0$.
2: **while** $l\le L$ **do**
3: Calculate $B(K)=l\frac{B_{\max}}{L}$ and $F_D^*(B(K),K)=R_{\mathrm{DT}}(K)$.
4: **for** all possible channel state $\boldsymbol{\xi}(K)$ **do**
5: Solve equation (33) according to step 4–14 in Algorithm 3.
6: Record $\{\theta^*(K)\}$ in the entry corresponding to $\tilde{\boldsymbol{D}}(K)$.
7: **end for**
8: Calculate $\bar{F}^*\big(\tilde{\boldsymbol{D}}(K),K\big)$ according to (34).
9: Set $l=l+1$.
10: **end while**
11: Set $k=K$ and $l=0$.
12: **while** $k\ge 1$ **do**
13: $k=k-1$.
14: **while** $l\le L$ **do**
15: Calculate $B(k)=l\frac{B_{\max}}{L}$ and $F_D^*(B(k),k)=R_{\mathrm{DT}}(k)$.
16: **for** all possible channel state $\boldsymbol{\xi}(k)$, **do**
17: Solve equation (32) according to step 22–32 in Algorithm 3.
18: Record $\{\theta^*(k),B^*(k+1)\}$ in the entry corresponding to $\tilde{\boldsymbol{D}}(k)$.
19: **end for**
20: **if** $k>1$ **then**
21: Calculate $\bar{F}^*\big(\tilde{\boldsymbol{D}}(k),k\big)$ according to (34).
22: **end if**
23: Set $l=l+1$.
24: **end while**
25: **end while**

Note that we can establish the look-up table offline before transmission. After the establishment of the look-up table, we can implement joint TS operation and power allocation online for the WPRN. We present the involved procedure in Algorithm 5. In this algorithm, the input includes the look-up table and the network state $\boldsymbol{D}(k)=\{\boldsymbol{g}(k),B(k)\}$. Therefore, Algorithm 5 is based on causal CSI, and thus it is a practical algorithm.

In step 6 of Algorithm 5, we solve problem (19) to obtain the joint TS operation and power allocation strategy. This is because the inner problem of problem (29) is the same as (19).

Algorithm 5 Online Joint Time Switching and Power Allocation Algorithm.

1: Map the CSI $\boldsymbol{g}(k)$ to $\boldsymbol{\xi}(k)$ to obtain $\tilde{\boldsymbol{D}}(k)$.
2: Search for the entry corresponding to $\tilde{\boldsymbol{D}}(k)$, and read $\theta^*(k)$ from the located entry.
3: **if** $\theta^*(k) = 0$ **then**
4: The source sends information directly to the destination and the relay harvests energy from the RF signals.
5: **else**
6: Read $B^*(k+1)$ from the located entry,
7: Let $B(k+1) = B^*(k+1)$ and solve problem (19) to achieve the optimal $\bar{\Xi}^*(k)$,
8: The source and the relay cooperatively send information to the destination based on the optimal $\bar{\Xi}^*(k)$.
9: **end if**

4.4. Complexity analysis

The computational complexity of Algorithm 5 is mainly from solving problem (19), which is implemented by Algorithm 2. In Algorithm 2, the computational complexity is from implementing the two-layer golden section search technique. For the golden section search technique, we denote the computational complexity as X. Thus, the computational complexity to implement two-layer golden section search is $\mathcal{O}\{X^2\}$, which indicates that Algorithm 5 has low computational complexity.

Note that the offline algorithm, i.e., Algorithm 3, has higher computational complexity than the online algorithm, i.e., Algorithm 5. This is because the computational complexity of Algorithm 3 is mainly caused by solving problem (17) for $(L+1)$ discrete energy states and problem (18) for $(L+1)$ discrete energy states over $(K-1)$ consecutive frames. To solve problem (17) or (18), Algorithm 2 is required to be executed. Thus, the computational complexity of Algorithm 3 is $\mathcal{O}\{(L+1)KX^2\}$. Nevertheless, Algorithm 3 can be implemented offline by a general-purpose computer, which has higher computational capacity than the wireless nodes in the WPRN, thus the higher computational complexity can be easily tackled in practice.

5. Simulation results

We evaluate the performance of our proposed scheme by computer simulations in this section. We assume that the time-varying i.i.d. AWGN channel has zero mean and unit variance. The source-to-destination distance is $d_3 = 10m$, the source-to-relay distance is $d_1 = \rho d_3$ $(0 < \rho < 1)$ and the relay-to-destination distance is $d_2 = d_3 - d_1$. We assume that the channel between the source and the relay and the channel between the relay and the destination follow the line-of-sight propagation, thus we set the power path-loss exponents as $\eta = 2$. Meanwhile, we assume that there are obstacles between the source and the destination, thus we set the power path-loss exponent as $\eta = 4$. As in [26], we adopt a path-loss model which is expressed as $\eta(10 + 10\log_{10} d_i)$, where $i \in \{1, 2, 3\}$. We set the power of AWGN as $\sigma_2^2 = \sigma_3^2 = 2 \times 10^{-9}$W, the energy utilization efficiency as $\tau = 0.8$, $B(1) = 0$, the number of frames in one period as $K = 10$ and the duration of one frame as $T_f = 10\mu s$. Moreover, we set the number of energy states as $L = 20$ and let $B_{\max} = 2E_h = 2\tau P_1 \tilde{g}_1$, where $\tilde{g}_1$ is the mean of g_1. In the follows, we refer to the proposed scheme as the practical scheme which is implemented by Algorithm 5.

To show the superior performance achieved by our proposed scheme, we compare the throughput achieved by our proposed scheme with that achieved by the existing schemes in Figs. 5 and 6. In Fig. 5, we set $P_1 = 20$dBm and show the achieved throughput when the relay location varies. Meanwhile, in Fig. 6, we set $\rho = 0.5$ and show the achieved throughput when the transmit power of the source, i.e., P_1, varies. From both the two figures, it can be seen that our proposed scheme outperforms the conventional TSR-based HTF scheme, the direction transmission scheme and the ATF scheme. Moreover, it can be seen that the gap between the throughput achieved by the proposed practical scheme and its upper bound, which is achieved by Algorithm 3, is very small. Furthermore, to reveal the advantages of enabling the relay to harvest energy in CT mode, we illustrate the throughput achieved by a simple scheme without EH in CT mode, where we fix $\lambda_1(k) = 0$ while solving problem (19), which indicates that the relay harvests energy only when the WPRN operates in DT mode. It can be seen from Figs. 5 and 6 that our proposed scheme outperforms the proposed simple scheme, which indicates that the throughput performance can be further improved when the relay is enabled to harvest energy in CT mode.

In Fig. 7, we show the impact of the number of frames, i.e., K, in one period on the throughput performance in our proposed scheme., where $\rho = 0.5$ and $P_1 = 20$dBm. From Fig. 7, it can be found that the achieved throughput can be improved as K increases. The reason is that more wireless channel variations can be utilized as K becomes larger. Specially, it can be found in Fig. 7 that the achieved throughput increases distinctly when K is small and becomes steady when K is large. Note that larger K results in more entries in the look-up table, which indicates that higher

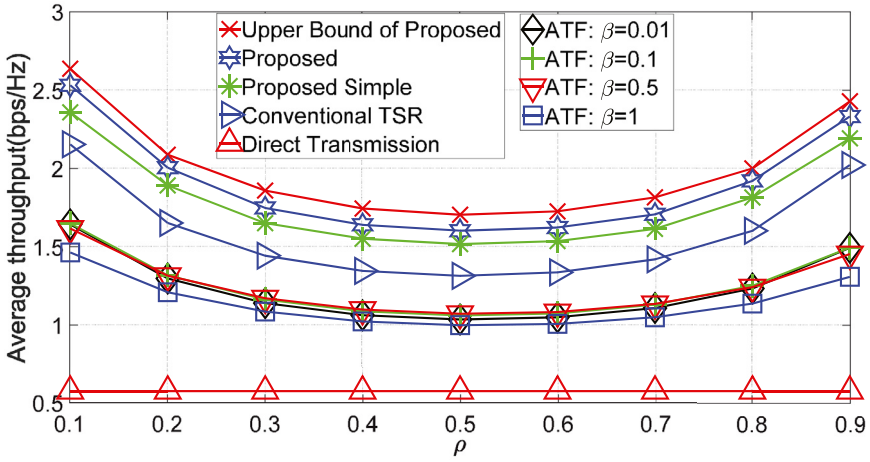

Fig. 5. The average throughput achieved by different schemes when the relay locates differently.

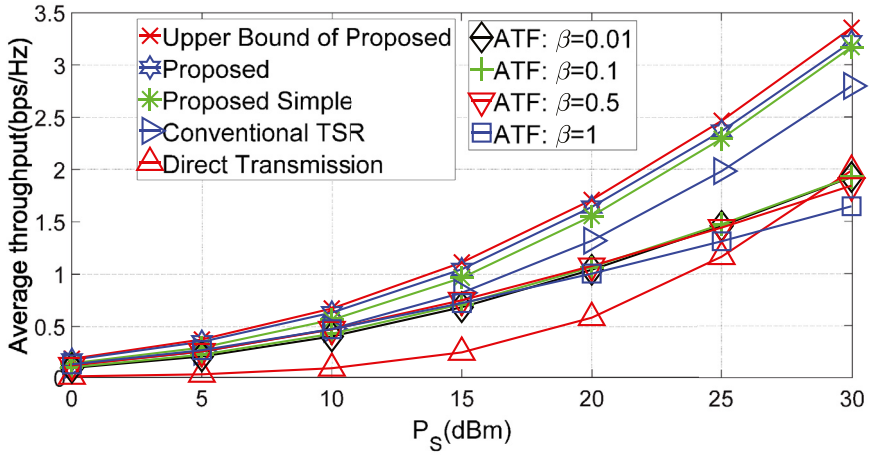

Fig. 6. The average throughput achieved by different schemes when the transmit power of the source varies.

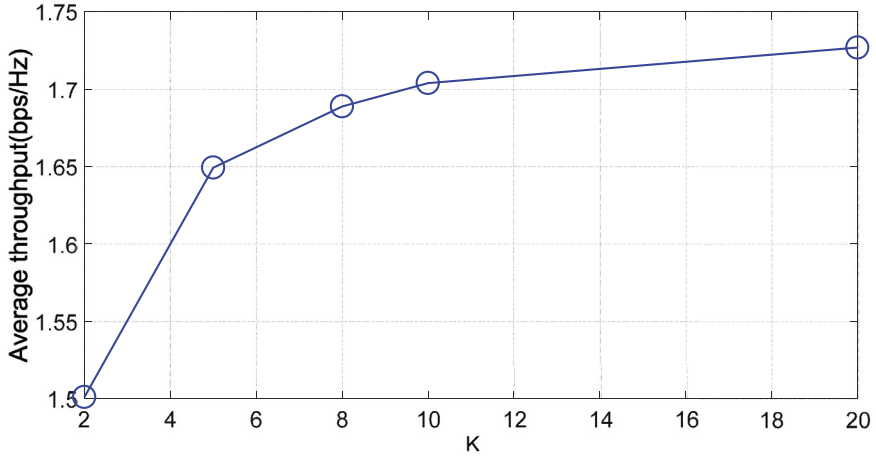

Fig. 7. Average throughput achieved by our proposed scheme with different K values.

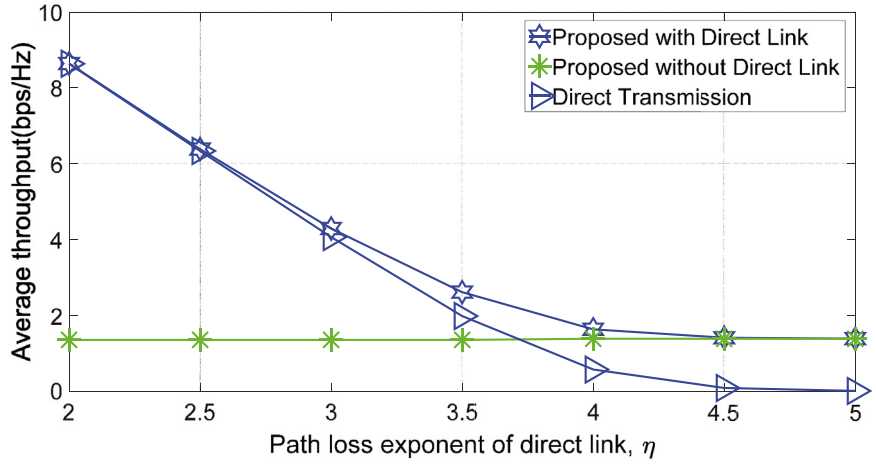

Fig. 8. The impact of the direct link on the throughput performance.

computational complexity is required for the establishment of the look-up table. Therefore, K should be set as a medium value when implementing the proposed scheme in practice, which is the reason why we set $K = 10$ in the other simulations in this paper.

Fig. 8 shows the achieved throughput by varying the path loss exponent of the direct link when implementing Algorithm 5. To verify the impact of the direct link on throughput performance, we also illustrate the achieved throughput where the direct link is ignored and the throughput achieved by direct transmission in Fig. 8. From Fig. 8, it can be found that the throughput can be significantly improved by considering the direct link, especially when the path loss exponent, i.e., η, of the direct link varies from 2 to 4. Meanwhile, it can be found that the deployment of EH relay can increase the throughput since the throughput achieved by the

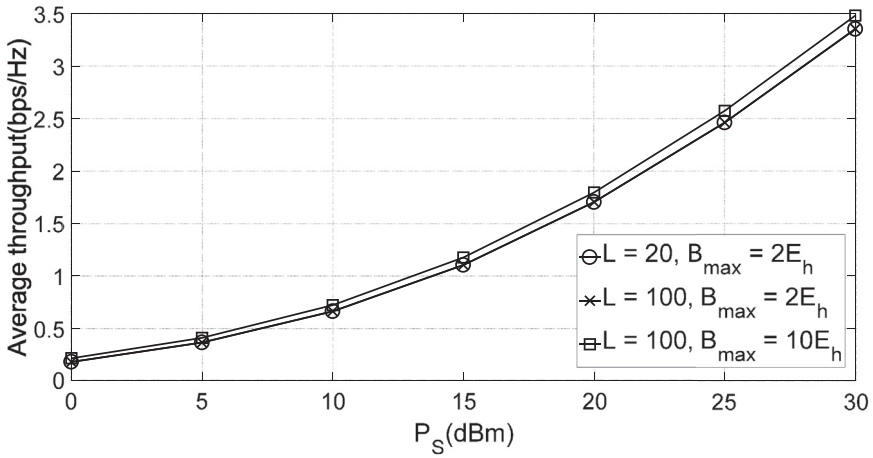

Fig. 9. Average throughput achieved by our proposed scheme with different $B_{\max}$ values and L values.

proposed scheme with direct link is higher than that achieved by direct transmission, especially when the path loss exponent of the direct link varies from 3 to 5.

According to the analysis in previous sections, we have quantized the energy state of the rechargeable device into discrete values with the step length $\frac{B_{\max}}{L}$ in our proposed scheme. Clearly, the smaller the step length and the larger $B_{\max}$ are, the more accurate (or higher) the throughput can be achieved. Therefore, to evaluate the impact of the values of $B_{\max}$ and L on the performance in our proposed scheme, we show the throughput by setting $B_{\max}$ and L with different values in Fig. 9. From Fig. 9, it can be found that when $B_{\max} = 2E_h$, the throughput achieved by setting $L = 20$ is almost the same as that achieved by setting $L = 100$. Moreover, it can be found in Fig. 9 that although the throughput can be improved by increasing $B_{\max}$ from $2E_h$ to $10E_h$ and setting $L = 100$, the achieved throughput gains are small. Note that as the number of energy states increases, the computational complexity of the establishment of the look-up table increases. Therefore, we set $B_{\max} = 2E_h$ and $L = 20$ in the previous simulations.

6. Conclusions

In this paper, we investigated the WPRN with a direct link in order to improve the throughput performance by the joint optimization of time switching and power allocation for multiple frames. By considering the DT and CT network operation modes and the HSC energy consumption model, we formulated the problems to maximize throughput for both the cases of full CSI and causal CSI. First, we used dynamic programming and problem decomposition techniques to derive an algorithm when solving the problem for the case of full CSI. This provided a benchmark of achievable throughput under the HSC model. Motivated by the derivation of the results for the case of full CSI and by using the FSMC channel model, we then solved the problem for the case of causal CSI and proposed an online and low-complexity algorithm to achieve joint time switching and power allocation. Our simulation results verified our scheme achieved the better performance in terms of throughput over a period of time which was for transmissions of consecutive multiple frames.

Note that although this paper focuses on a WPRN with a single reply (as those in [10–24]), the results may provide insights into the design of more complex WPRNs. When multiple relays exist, we can further enhance the network performance by jointly optimizing the power allocations at the relays while the relays operate in CT mode, which is a more complicated problem. Therefore, the design of optimization scheme for the multi-relay WPRN is an interesting future work

Declaration of Competing Interest

The authors declare that they have no known competing financial interests or personal relationships that could have appeared to influence the work reported in this paper.

Acknowledgments

This work was supported in part by the National Natural Science Foundation of China under Grant 61872098, the Natural Science Foundation of Guangdong Province under Grants 2017A030313363 and 2017A030310639, the Science & Technology Project of Guangdong Province under Grant 2016A010101032, the Science & Technology Project of Guangzhou City under Grant 201605030014 and the Academic Visiting Scholarship under the State Scholarship Fund of China.

Appendix A. Proof of Proposition 1

Proposition 1 consists of two parts. The first part is for the case of $g_3(k) \geq g_1(k)$, and the second part is for the case of $g_3(k) < g_1(k)$. Since $F_{\mathrm{D}}^*(B(k),k)$ and $F_{\mathrm{C}}^*(B(k),k)$ can be obtained by substituting $\theta(k) = 0$ and $\theta(k) = 1$ into Eqs. (13) and (14), respectively, the second part can be easily verified by comparing the values of $F_{\mathrm{D}}^*(B(k),k)$ and $F_{\mathrm{C}}^*(B(k),k)$, where $k \in \mathcal{K}$. Therefore, we focus on the proof of the first part in the follows.

According to (14), we have $F^*(B(K),K) = F_{\mathrm{D}}^*(B(K),K)$ when $\theta(K) = 0$ and $F^*(B(K),K) = F_{\mathrm{C}}^*(B(K),K)$ when $\theta(K) = 1$. Meanwhile, according to (13), we have $F^*(B(k),k) = F_{\mathrm{D}}^*(B(k),k)$ when $\theta(k) = 0$ and $F^*(B(k),k) = F_{\mathrm{C}}^*(B(k),k)$ when $\theta(k) = 1$, where $k \in \mathcal{K}^o$.

When $g_3(k) \geq g_1(k)$, according to the expression of $R_{\mathrm{CT}}(k)$ in (2), we obtain $R_{\mathrm{DT}}(K) \geq R_{\mathrm{CT}}(K)$ for any $\bar{\Xi}(K)$ and $R_{\mathrm{DT}}(k) \geq R_{\mathrm{CT}}(k)$ for any $\bar{\Xi}'(k)$. Since $R_{\mathrm{DT}}(K) \geq R_{\mathrm{CT}}(K)$ for any $\bar{\Xi}(K)$, we have $F_{\mathrm{D}}^*(B(K),K) > F_{\mathrm{C}}^*(B(K),K)$. Thus, the optimal $\theta^*(K)$ to problem (30) is $\theta^*(K) = 0$.

Let's consider the case of $k \in \mathcal{K}^o$. According to (15), we obtain $\tilde{B}(k+1) \geq B(k+1)$ when $k \in \mathcal{K}^o$. Meanwhile, the $F^*(\cdot)$ function in Eqs. (13) and (14) increases monotonically with $B(k)$. Therefore, we can obtain $F^*\big(\tilde{B}(k+1),(k+1)\big) \geq F^*(B(k+1),(k+1))$ when $k \in \mathcal{K}^o$. Moreover, when $g_3(k) \geq g_1(k)$, since $R_{\mathrm{DT}}(k) \geq R_{\mathrm{CT}}(k)$ for any $\bar{\Xi}'(k)$, we can obtain that $F_{\mathrm{D}}^*(B(k),k) > F_{\mathrm{C}}^*(B(k),k)$, which results in that $\theta^*(k) = 0$. To this end, the proof of Proposition 1 is completed.

Appendix B. Proof of Lemma 1

We prove this lemma by reductio ad absurdum. Suppose that at optimality we have

$$\lambda_2(k)R_1(k) < [\lambda_1(k)+\lambda_2(k)]R_3(k)+\lambda_3(k)R_c(k). \quad (35)$$

In this case, we can decrease $\lambda_3(k)$ such that the inequality in (35) and the constraint in problem (21), i.e., (18b) are still satisfied. As we decrease $\lambda_3(k)$, we can increase the value of $\lambda_1(k)+\lambda_2(k)$. Since $\lambda_1(k)$ is given, the left hand side of (35), i.e., $\lambda_2(k)R_1(k)$, increases. As a result, the objective function in problem (21) increases. This contradicts our initial assumption that the achieved solution is at optimality.

Appendix C. Proof of Proposition 2

We prove this proposition by reductio ad absurdum. Suppose that at optimality we have $T_f\lambda_3(k)p_2(k) < W(k)$. Then, we can increase $p_2(k)$ such that $T_f\lambda_3(k)p_2(k) = W(k)$. As a result, the left-hand side (23), i.e., $\lambda_2(k)R_1(k)$, does not decrease, and the right-hand side, i.e., $[\lambda_1(k)+\lambda_2(k)]R_3(k)+\lambda_3(k)R_c(k)$, increases. From Lemma 1, we obtain that at optimality the right-hand side of (23) determines the optimal value of the objective function in (21). Therefore, the optimal value of problem (21) increases. This contradicts our initial assumption that the achieved solution is at optimality.

References

[1] Y. Xu, C. Shen, Z. Ding, X. Sun, S. Yan, G. Zhu, Z. Zhong, Joint beamforming and power-splitting control in downlink cooperative SWIPT NOMA systems, IEEE Trans. Signal Process. 65 (18) (2017) 4874–4886.

[2] C. Xu, C. Song, P. Zeng, H. Yu, Secure resource allocation for energy harvesting cognitive radio sensor networks without and with cooperative jamming, Comput. Netw. 141 (2018) 189–198.

[3] I. Ahmed, M.M. Butt, C. Psomas, A. Mohamed, I. Krikidis, M. Guizani, Survey on energy harvesting wireless communications: challenges and opportunities for radio resource allocation, Comput. Netw. 88 (2015) 234–248.

[4] G. Zhang, J. Xu, Q. Wu, M. Cui, X. Li, F. Lin, Wireless powered cooperative jamming for secure OFDM system, IEEE Trans. Veh. Technol. 67 (2) (2018) 1331–1346.

[5] Q. Li, Q. Zhang, J. Qin, Secure relay beamforming for SWIPT in amplify-and–forward two-way relay networks, IEEE Trans. Veh. Technol. 65 (11) (2016) 9006–9019.

[6] D. Mishr, G.C. Alexandropoulos, S. De, Transmit precoding and receive power splitting for harvested power maximization in MIMO SWIPT systems, IEEE Trans. Green Commun. Netw. 2 (3) (2018) 774–786.

[7] D. Mishra, G.C. Alexandropoulos, S. De, Energy sustainable IoT with individual QoS constraints through MISO SWIPT multicasting, IEEE Internet Things J. 5 (4) (2018) 2856–2867.

[8] D. Mishra, G.C. Alexandropoulos, S. De, Jointly optimal spatial channel assignment and power allocation for MIMO SWIPT systems, IEEE Wireless Commun. Lett. 7 (2) (2018) 214–217.

[9] D. Mishra, S. De, G.C. Alexandropoulos, D. Krishnaswamy, Energy-aware Mode Selection for Throughput Maximization in RF-Powered D2D Communications, in: IEEE Global Communications Conference (GLOBECOM), Singapore, 2017.

[10] A.A. Nasir, X. Zhou, S. Durrani, R.A. Kennedy, Relaying protocols for wireless EH and information processing, IEEE Trans. Wireless Commun. 12 (7) (2013) 3622–3636.

[11] Y. Feng, V.C.M. Leung, F. Ji, Performance study for SWIPT cooperative communication systems in shadowed nakagami-*m* fading channels, IEEE Trans. Wireless Commun. 17 (7) (2018) 1199–1211.

[12] G. Amarasuriya, E.G. Larsson, H.V. Poor, Wireless information and power transfer in multiway massive MIMO relay networks, IEEE Trans. Wireless Commun. 15 (6) (2016) 3837–3855.

[13] M. Mohammadi, B.K. Chalise, H.A. Suraweera, C. Zhong, G. Zheng, I. Krikidis, Throughput analysis and optimization of wireless-powered multiple antenna full-duplex relay systems, IEEE Trans. Commun. 64 (4) (2016) 1769–1785.

[14] Y. Zhang, J. Ge, E. Serpedin, Performance analysis of a 5g energy-constrained downlink relaying network with non-orthogonal multiple access, IEEE Trans. Wireless Commun. 16 (12) (2017) 8333–8346.

[15] G. Huang, W. Tu, Joint power splitting and power allocation for two-way OFDM relay networks with SWIPT, Comput. Commun. 124 (2018) 76–86.

[16] G. Huang, W. Tu, On opportunistic energy harvesting and information relaying in wireless-powered communication networks, IEEE Access 6 (2018) 55220–55233.

[17] F. Zeng, J. Xua, Y. Li, K. Li, L. Jiao, Performance analysis of underlay two-way relay cooperation in cognitive radio networks with energy harvesting, Comput. Netw. 142 (2018) 13–23.

[18] H. Shi, Y. Cai, D. Chen, J. Hu, W. Yang, W. Yang, Physical layer security in an untrusted energy harvesting relay network, IEEE Access (2018), doi:10.1109/ACCESS.2019.2897357.

[19] O.T. Demir, T.E. Tuncer, Robust optimum and near-optimum beamformers for decode-and-forward full-duplex multi-antenna relay with self-energy recycling, IEEE Trans. Wireless Commun. 18 (3) (2019) 1566–1580.

[20] C. In, H.M. Kim, W. Choi, Achievable rate-energy region in two-way decode-and-forward energy harvesting relay systems, IEEE Trans. Commun. (2019), doi:10.1109/TCOMM.2019.2901783.

[21] R. Malik, M. Vu, Optimal transmission using a self-sustained relay in a full-duplex MIMO system, IEEE J. Sel. Areas Commun. 37 (2) (2019) 374–390.

[22] C. Zhai, Z. Yu, X. Wang, High-efficient cooperative relaying with wireless powered source and relay, Comput. Netw. 152 (2019) 199–209.

[23] X. Di, K. Xiong, P. Fan, H.C. Yang, Simultaneous wireless information and power transfer in cooperative relay networks with rateless codes, IEEE Trans. Veh. Technol. 66 (4) (2017) 2981–2996.

[24] Z. Li, H. Chen, Y. Li, B. Vucetic, Incremental Accumulate-then-Forward Relaying in Wireless Energy Harvesting Cooperative Networks, in: IEEE Global Communications Conference (GLOBECOM), Singapore, 2017.

[25] F. Yuan, Q.T. Zhang, S. Jin, H. Zhu, Optimal harvest-use-store strategy for energy harvesting wireless systems, IEEE Trans. Wireless Commun. 14 (2) (2015) 698–710.

[26] X. Zhou, R. Zhang, C.K. Ho, Wireless information and power transfer: architecture design and rate-energy tradeoff, IEEE Trans. Wireless Commun. 61 (11) (2013) 4754–4767.

[27] M. Zhao, J. Zhao, W. Zhou, J. Zhu, S. Zhang, Energy efficiency optimization in relay-assisted networks with energy harvesting relay constraints, China Commun. 12 (2) (2015) 84–94.

[28] A. Molisch, N. Mehta, J. Yedidia, J. Zhang, Performance of fountain codes in collaborative relay networks, IEEE Trans. Wireless Commun. 6 (11) (2007) 4108–4119.

[29] A. Ravanshid, L. Lampe, J.B. Huber, Dynamic decode-and-forward relaying using raptor codes, IEEE Trans. Wireless Commun. 10 (5) (2011) 1569–1581.

[30] W.J. Huang, Y.W.P. Hong, C.C.J. Kuo, Lifetime maximization for amplify-and–forward cooperative networks, IEEE Trans. Wireless Commun. 7 (5) (2008) 1800–1805.

[31] P. Sadeghi, R. Kennedy, P. Rapajic, R. Shams, Finite-state Markov modeling of fading channels: survey of principles and applications, IEEE Signal Process. Mag. 25 (5) (2008) 57–80.

[32] D.P. Bertsekas, Dynamic Programming and Optimal Control, MA: Athena Scientific, Belmont, 1995. Volume 1.

Gaofei Huang is an associate professor in the Department of Electronics and Communication Engineering in Guangzhou University, P.R. China. He received his M.S. and Ph.D degrees from Sun Yat-sen University, P.R. China, in 2004 and 2012, respectively. His current research interests include energy-harvesting wireless networks, resource allocations in next-generation wireless networks and cross-layer design of wireless networks.

Wanqing Tu is a senior lecturer in the Department of Computing Science at The University of Auckland, New Zealand. She received her PhD from the Department of Computer Science at the City University of Hong Kong. Her research interests include wireless multi-hop communications, multimedia communications, QoS/QoE, IoT, overlay networks, and distributed computing. She received an IRCSET Embark Initiative Postdoctoral Research Fellowship. She received one Best Paper Award in 2005. She is a Senior Member of the IEEE.